JOURNAL OF PROPULSION AND POWER
Vol. 10, No. 5, Sept.–Oct. 1994

Theoretical vs Experimental Rotordynamic Coefficients of Incompressible Flow Labyrinth Seals

E. A. Baskharone* and A. Ghali†
Texas A&M University, College Station, Texas 77843

A detailed finite element-based perturbation analysis, initially developed for straight annular seals, is extended to the labyrinth seal rotordynamics problem. This particular seal category is frequently used in turbopumps, such as those of the Space Shuttle Main Engine, for its effectiveness as a leakage control device. The same seal configuration is also known to produce a net destabilizing force, which stems from the fluid/rotor interaction mechanism. The general objective here is to assess the effect of a design parameter, namely the number of tooth-to-tooth chambers, on the seal rotordynamic characteristics and relative stability. To this end, two representative cases of teeth-on-rotor labyrinth seals are selected for the purpose of comparison. The chosen seals share the same tooth-to-tooth chamber geometry, but are composed of one and five such chambers. The computed rotordynamic coefficients are compared to an existing set of experimental measurements concerning the same two seal configurations. The final outcome of the study is consistent with the general belief that labyrinth seals impart a rotordynamically destabilizing effect. In terms of relative stability, however, the five-chamber seal configuration offers less of this destabilizing effect, by comparison.

Nomenclature

C = direct damping coefficient of the fluid/rotor interaction
c = cross-coupled damping coefficient
F_r = radial component of the fluid-induced force
F_r^* = $\partial F_r/\partial \varepsilon$
F_θ = tangential component of the fluid-induced force
F_θ^* = $\partial F_\theta/\partial \varepsilon$
f = whirl frequency ratio
h = seal clearance
K = direct stiffness coefficient of the fluid/rotor interaction
k = cross-coupled stiffness coefficient
p = static pressure
p_i = seal-inlet static pressure
r = radius
r_i = inner radius of the labyrinth seal
V_z = axial velocity component
V_θ = tangential velocity component
ε = lateral eccentricity of the rotor axis
ρ = density
Ω = whirl frequency
ω = rotor operating speed

Introduction

LABYRINTH seals are generally regarded as efficient leakage-control devices in turbomachinery applications (Fig. 1). Since leakage flow is considered one of the primary loss mechanisms and, subsequently, performance degradation in turbomachines, much of the numerical studies on seals have been focused on this particular seal category. Among those are the computational leakage models by Stoff[1] and Rhode et al.[2] for incompressible flow applications. Compressible flow labyrinth seal models, for gas turbine applications, have also been devised (e.g., Wittig et al.[3] and, more recently, Rhode and Hibbs[4]).

Experimental measurements and flow-visualization studies in labyrinth seals have also been reported in the literature. Examples of these include the laser Doppler anemometer measurements by Wittig et al.,[3] the flow visualization study by Iwatsubo and Kawai,[5] and the discharge coefficient measurements by Wittig et al.[3] The complexity of the flow structure in labyrinth seals has also encouraged researchers to devise, and continually update, empirical correlations.[6]

Despite the performance improvements attained through the utilization of labyrinth seals, serious fluid-induced vibrations have been attributed to them by many rotordynamicists. Among those, Alford[7] was the first to point out the destabilizing effects of labyrinth seals. Iwatsubo and Kawai[5] later reported significantly poor direct damping coefficients for a hydraulic labyrinth seal under a matrix of different operating conditions. In a comparative study involving several seal categories, Childs and Elrod[8] also concluded that the flow swirl at the labyrinth seal inlet station would make a bad rotordynamic situation even worse, and that an effective swirl brake would be required in this case.

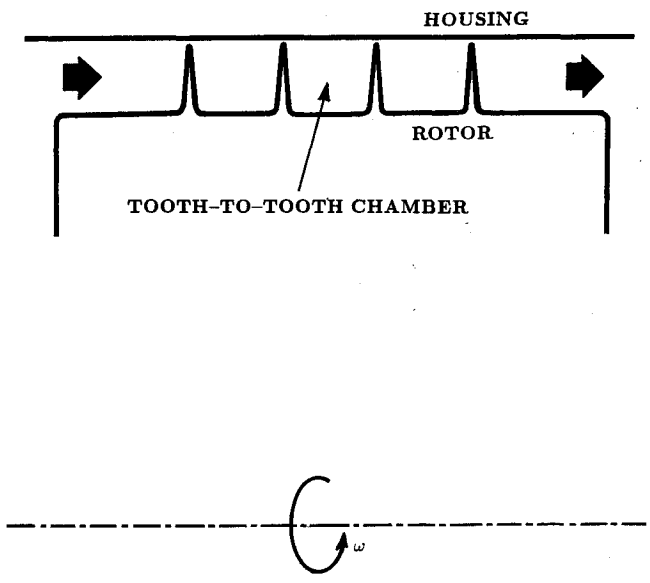

Fig. 1 Schematic of a typical labyrinth seal.

Received April 13, 1993; revision received Feb. 16, 1994; accepted for publication Feb. 17, 1994.

*Associate Professor, Department of Mechanical Engineering. Member AIAA.
†Graduate Research Assistant, Department of Mechanical Engineering.

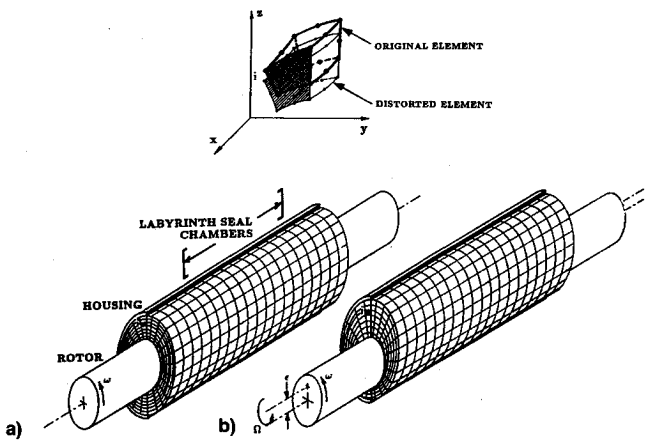

Fig. 2 Distortion of the rotor-to-housing finite element assembly as a result of the rotor eccentricity: a) centered and b) whirling rotor operator modes.

Recent theoretical developments in this area have generally been either too simplified to account for real flow effects in labyrinth seals, or so tailored as to handle simple geometries and/or uniform lateral eccentricity of the whirling rotor. Under the first category are the "one-volume" models by Iwatsubo[9] and that by Childs and Scharrer.[10] To the author's knowledge the first attempt to apply rigorous computational fluid dynamics tools, within the framework of a perturbation approach, was that by Nordmann and Weiser.[11] This finite difference-based model is based on the transformation of the entire rotor-to-housing computational domain to a fictitious frame of reference whereby the rotor eccentricity (assumed uniform along the seal axis) is eliminated. Despite the apparent generality and complex nature of this approach, the method is practically limited to rectangular tooth-to-tooth chambers, and is conceptually incapable of addressing rotor excitations in the form of conical whirl, which would be of serious consequence for long seals with appreciable streamwise pressure differential.

The current perturbation model is a versatile predictive tool, which is based on what we generically termed the "virtually" deformable finite element concept. Theoretical details of this model were documented by Baskharone and Hensel,[12] and a sample case of a straight annular seal successfully analyzed.[13] Versatility of this model was also demonstrated by analyzing, as interrelated, the cylindrical and conical whirl of a straight annular seal rotor.[14] The present study illustrates another versatility aspect of the perturbation model, namely that of the seal geometry arbitrariness. The study addresses both the traditional difficulty of analyzing the flow past a sequence of high aspect-ratio cavities, normally found in labyrinth seals, as well as the task of classifying, as restoring or aggravating, the fluid reaction forces due to excitations of the rotor axis (Fig. 2).

Computational Development

The perturbation procedure is initiated by computing the "zeroth-order" flowfield (Fig. 1), which is clearly axisymmetric. The boundary conditions here consist of prescribed inlet profiles of the axial, radial, and tangential velocity components. At the flow-discharge station, zero streamwise derivatives of these components are imposed, and the exit static pressure specified. Details of the flow-governing equations, turbulence closure, and finite element formulation of this relatively simple problem were all discussed by Baskharone and Hensel,[13] where a test case involving a straight annular seal was comprehensively covered. Comparison of the computed through-flow and swirl velocity profiles in the rotor-to-housing passage with the experimental data previously reported by Morrison et al.,[15] was also presented, and the agreement between the two sets of data was encouraging. For instance,

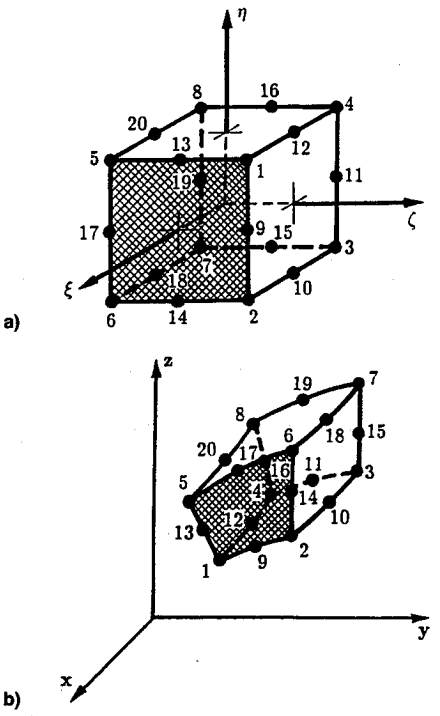

Fig. 3 Quadrilateral curve-sided isoparametric finite element: a) local and b) physical frame of reference.

the maximum difference between the computed and measured values of the through-flow velocity component was approximately 13% for all computational nodes in the entire clearance gap.

The centered-rotor flow solution, referenced above, was used in the current study as input to the perturbation analysis phase of the computational procedure. In this phase, the rotor-to-housing computational domain is discretized using the 20-noded curve-sided isoparametric finite element shown in Fig. 3. Devised by Baskharone and Hensel,[12] the perturbation model here is based on what was generically termed the virtually deformable finite element concept, where the perturbed flow equations emerge from expansion of the finite element equations in terms of the rotor eccentricity ε. Since no circumferential pattern is preimposed on the perturbations of the flow properties, the problem at this point shifts to the fully three-dimensional type, as the rotor eccentricity destroys the flow axisymmetry (Fig. 2). Simultaneously, the flow problem is cast in a rotating-translating frame of reference, which is attached to the whirling rotor at all times (Fig. 2) in order to eliminate the time dependency of the flowfield in this case.

Results and Discussion

Two labyrinth seals, composed of the same tooth-to-tooth chamber geometry, but different in the number of chambers, were selected for this study. These one- and five-chamber hydraulic seals were the subject of a flow visualization study and rotordynamic testing by Iwatsubo and Kawai.[5] The choice of these seal configurations was intended to both validate the computational model for this problem category, as well as illustrate major differences in the rotordynamic characteristics as a result of significantly varying the number of chambers. A rigorous parametric study concerning the effects of this geometrical aspect would have been computationally expensive and have little impact on the final conclusions. As for the seal operating conditions, a seal-inlet pressure and rotor speed of 147 kPa and 3.7 Hz, respectively, were arbitrarily chosen from the experimental matrix of operating conditions. The finite element model created for the two seal configurations are shown in Figs. 3 and 4, respectively. The discretization unit in these two figures is a biquadratic curve-sided element of the Lagrangian type. The process of generating

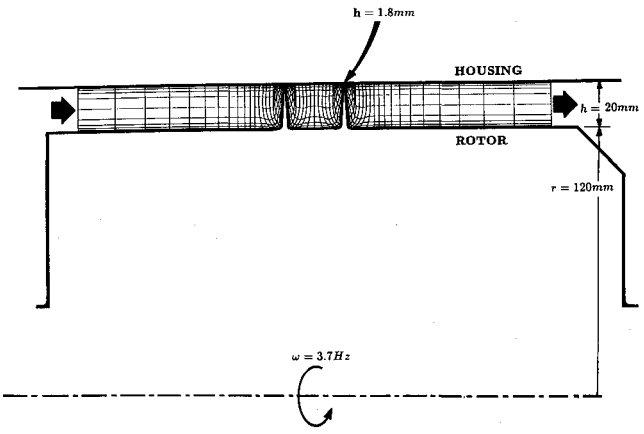

Fig. 4 Finite element model of the single-chamber seal configuration.

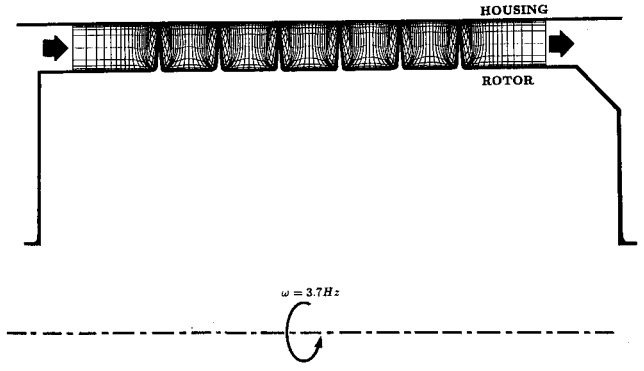

Fig. 5 Finite element model of the five-chamber seal configuration.

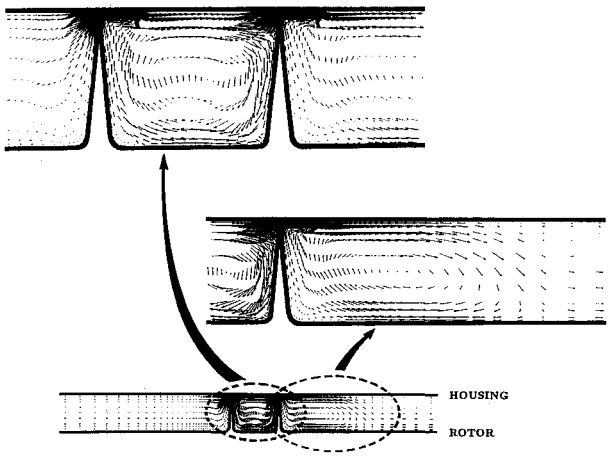

Fig. 6 Vector plot of the meridional velocity component for the centered-rotor operation mode of the single-chamber seal configuration.

finite element grids such as these was largely automated, and the level of near-wall refinement in the preprocessing segment of the computational procedure was made totally arbitrary. This capability made it possible to conduct a preliminary numerical "experimentation" study of grid optimization for the centered-rotor (axisymmetric) flow solution. The finite element grids in Figs. 4 and 5 are the outcome of this early study, where a careful compromise was made between the numerical accuracy, on one hand, and the consumption of computational resources, on the other.

Centered-Rotor Flowfield

Figures 6–8 show the centered-rotor flow solution for the one-chamber seal configuration. This solution constitutes the zeroth-order flowfield in the current perturbation analysis. First, the meridional flow behavior is shown in Fig. 6, with enlarged segments of the computational domain to clarify the flow recirculation within the tooth-to-tooth chamber and the vorticity breakdown in the dump region downstream from the chamber. The flow pattern in this figure was qualitatively compared to that resulting from a flow visualization study by Iwatsubo and Kawai,[5] and the major features of the computed flow pattern were found to be consistent with the experimental findings.

The swirl velocity contours, throughout the computational domain, are shown in Fig. 7. The swirl velocity V_θ in this figure is nondimensionalized using the average inlet through-flow velocity component V_{zi}. Note that the figure shows no inlet preswirl, which was enforced as a boundary condition in consistency with the seal-inlet conditions in the test rig.[5] Also note the swirl-velocity boundary-layer profile development over the rotor surface. As seen in the figure, the swirl velocity near the housing surface appears in the tooth-to-tooth chamber region, and steadily declines, over the housing, away from the chamber, up to the location where the flow recirculation zone, downstream from the second tooth (Fig. 6), ends. In viewing the swirl velocity distribution near the seal inlet station, the reader is reminded that the lack of preswirl in this test case (Fig. 7) is in no way a built-in assumption in the current computational model, but rather, is part of the inlet boundary conditions given by Iwatsubo and Kawai.[5]

Figure 8 shows a contour plot of the static pressure $\bar{p}$, with an enlarged view of the tooth-to-tooth seal chamber. The nondimensional pressure $\bar{p}$ in this figure is defined as follows:

$$\bar{p} = \frac{(p - p_i)}{0.5\rho V_{zi}^2}$$

where p and p_i are the local and seal-inlet static pressures, respectively, ρ is the fluid density, and V_{zi} is the average through-flow velocity at the seal inlet station. Note that the upstream side of the second tooth is exposed to a rather high pressure near the housing, despite the fact that the center of the low-pressure island is closer to that tooth.

Assessment of the centered-rotor flow solution (Figs. 6–8) was made in light of the results obtained by Rhode and Hibbs[4] using a fully elliptic, finite difference flow model for a single-cavity seal. Comparison between the two sets of results is shown in Fig. 9, where the nondimensionalized through-flow velocity and static pressure distributions along the midchamber line are displayed. Examination of this figure reveals a notable agreement between the two sets of results, both in trends and magnitudes, despite the obvious geometrical differences in the tooth geometry, by reference to Fig. 4, and the chamber aspect ratio.

The centered-rotor flowfield corresponding to the five-chamber seal configuration is shown in Figs. 10–12, with particular emphasis on the flow structure in the first and last chambers. Examination of Fig. 10 reveals that the center of the cavity recirculatory motion gradually moves from the cavity center towards the tooth pressure side as the flow progresses from one cavity to the next. The most significant difference between the swirl velocity distribution in Fig. 11 and that of the single-chamber seal (Fig. 7) is the continuous rise in the magnitude of this velocity component in the through-flow direction, by comparison. This characteristic simply means that the five-chamber seal gives rise to "elongated" flow trajectories over the last few chambers. One would expect, as a result, a substantial total pressure differential across these chambers, which is consistent with the known fact that the leakage-suppression capability of labyrinth seals is drastically enhanced by increasing the number of tooth-to-tooth chambers. As for the static pressure distribution in Fig. 12, it seems that the largest pressure increments occur across the first and last chambers. The computational procedure leading to the flow solution in Figs. 10–12 consumed a total of 22 CPU h on a 33-MHz MIPS workstation.

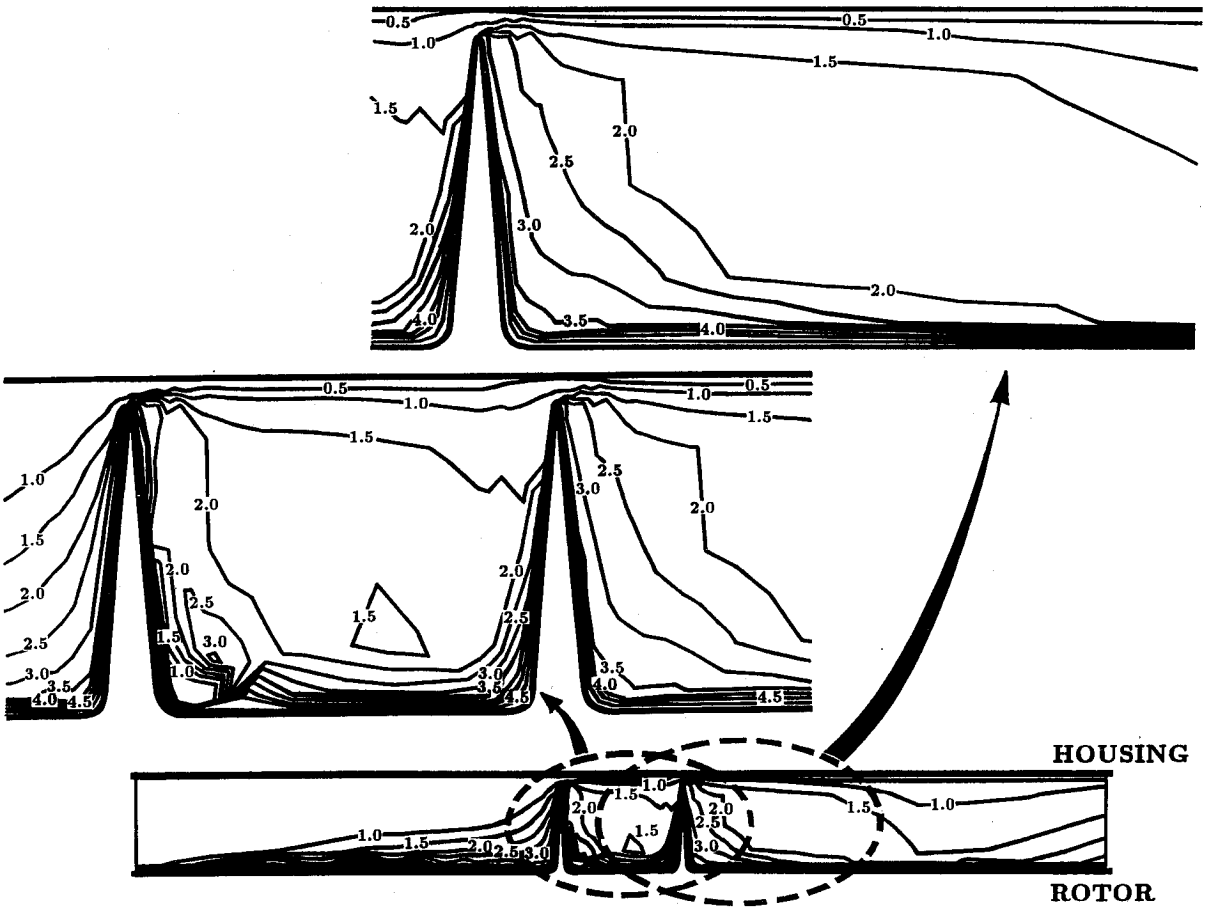

Fig. 7 Contour plot of the swirl velocity component for the centered-rotor operation mode of the single-chamber seal configuration.

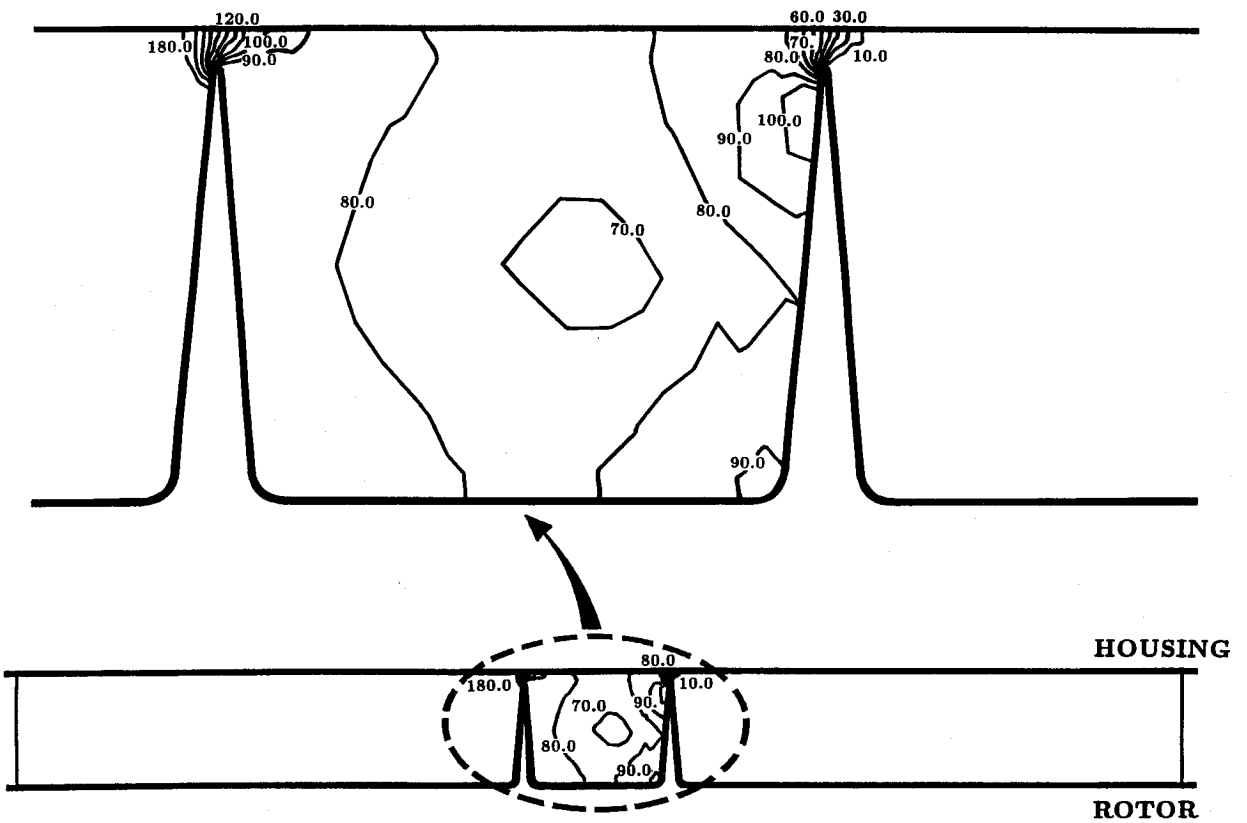

Fig. 8 Contour plot of the static pressure for the centered-rotor operation mode of the single-chamber seal configuration.

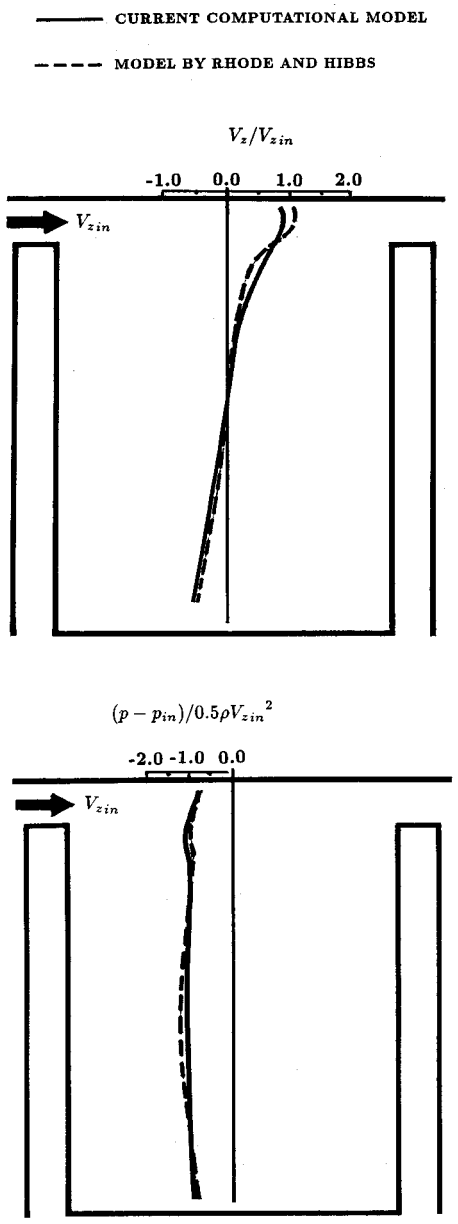

Fig. 9 Comparison of the midchamber axial velocity and static pressure distributions with those of Rhode and Hibbs.[4]

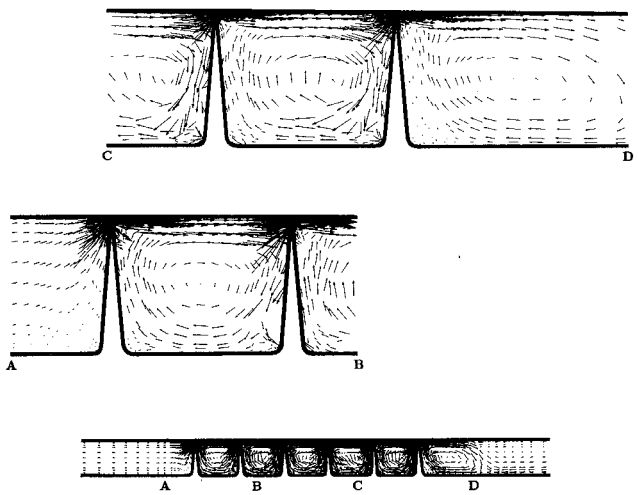

Fig. 10 Vector plot of the meridional velocity component for the centered-rotor operation mode of the five-chamber seal configuration.

Grid Dependency

As would naturally be anticipated, the perturbed flow resolution is dependent on the grid resolution, which as the domain three-dimensionality prevails, translates into the number of computational stations in the circumferential direction (Fig. 2). Investigation of this dependency was carried out by varying this number and repeatedly computing the fluid-exerted forces on the rotor for an arbitrarily chosen Ω that is identical to ω. Results of this preliminary step are shown in Fig. 13, where the fluid force components F_r^* and F_θ^* are obtained by integrating the rotor-surface pressure forces, upon resolution in the radial and tangential directions, over all of the contributing finite element boundaries.

The force trends in Fig. 13 suggest that the radial force is more sensitive to the tangential grid resolution by comparison. The figure also shows that changes in the force magnitudes become acceptably small as the tangential computational-station count approaches 11. Given the fact that F_r itself varies by as low as 2.7% by increasing the number of these computational stations from 10 to 11, and in an attempt to maintain a "manageable" CPU time consumption, the number was fixed at 11 thereafter.

Fluid-Induced Forces and Rotordynamic Coefficients

The trends of the fluid-exerted forces are shown in Fig. 14 for the five-chamber seal configuration over a range of the rotor whirl frequency between -200 and 200%, with the negative values representing backward whirl. A total of 21 whirl frequency ratios in this range were individually analyzed, with each ratio consuming approximately 13 h of CPU time on the IBM 3090-600 mainframe. The reassuring feature of the radial and tangential force trends in Fig. 12 is that each of them is more or less parabolic, a commonly known characteristic of seals in general. Of the two components in Fig. 14, the tangential force is exclusively responsible for aggravating or suppressing the rotor whirling motion. With this in mind, the impression one would have, by examining Fig. 14, is that of rotordynamic instability in the range of positive (forward) rotor whirl frequency between 0–20% of the rotor speed, judging by the positive tangential force in this range.

Determination of the Rotordynamic Coefficients

The procedure leading to these coefficients is initialized by considering a lateral eccentricity ε of the rotor axis, coupled with a circular whirling motion around the housing centerline, as shown in Fig. 15. In this case, the locus of the rotor axis can parametrically be described as follows[16]:

$$X = \varepsilon \sin(\Omega t), \qquad Y = \varepsilon \cos(\Omega t) \tag{1}$$

where X and Y are the eccentricity components of the rotor axis (Fig. 1), and t refers to time. Noting that the direction of Ω in Fig. 15 is negative, the rotor equation of motion can be written as follows:

$$-\begin{Bmatrix} \delta F_x \\ \delta F_y \end{Bmatrix} = \begin{bmatrix} K & -k \\ k & K \end{bmatrix} \begin{Bmatrix} X \\ Y \end{Bmatrix} + \begin{bmatrix} C & -c \\ c & C \end{bmatrix} \begin{Bmatrix} \dot{X} \\ \dot{Y} \end{Bmatrix} + \begin{bmatrix} M & -m \\ m & M \end{bmatrix} \begin{Bmatrix} \ddot{X} \\ \ddot{Y} \end{Bmatrix} \tag{2}$$

where

δF_x, δF_y = incremental changes in the rotor force components as a result of the rotor disturbance
M, m = inertia (or added mass) coefficients

Assuming cylindrical whirl around the housing centerline at a constant Ω, consider the position of the rotor axis shown

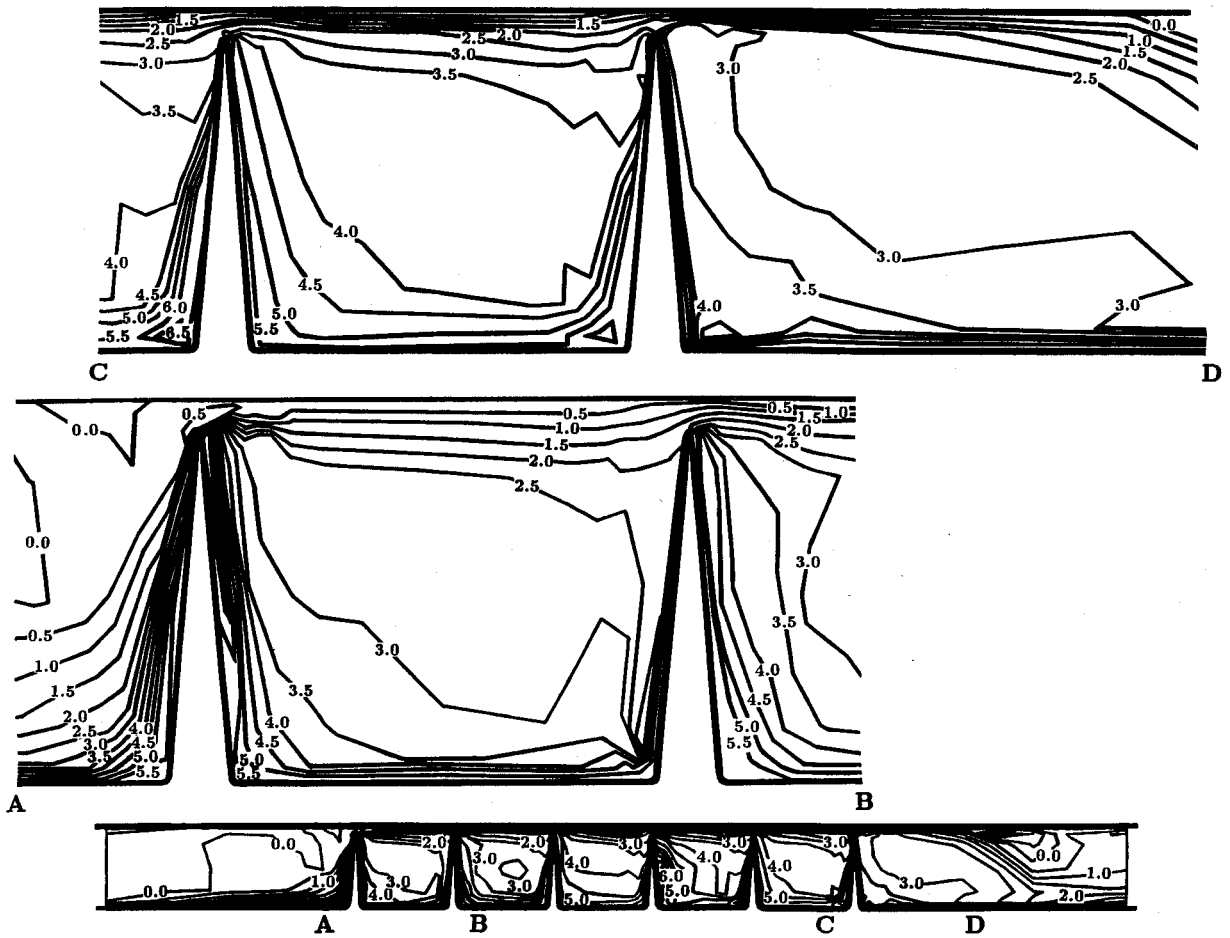

Fig. 11 Contour plot of the swirl velocity component for the centered-rotor operation mode of the five-chamber seal configuration.

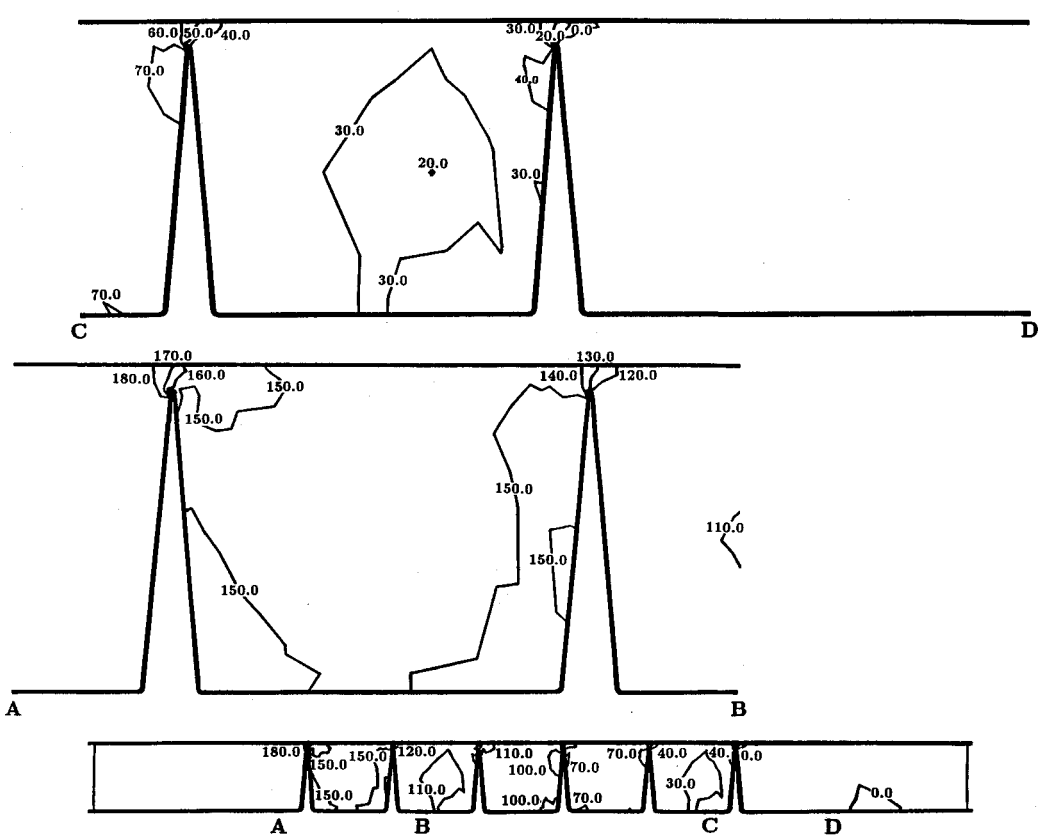

Fig. 12 Contour plot of the static pressure for the centered-rotor operation mode of the five-chamber seal configuration.

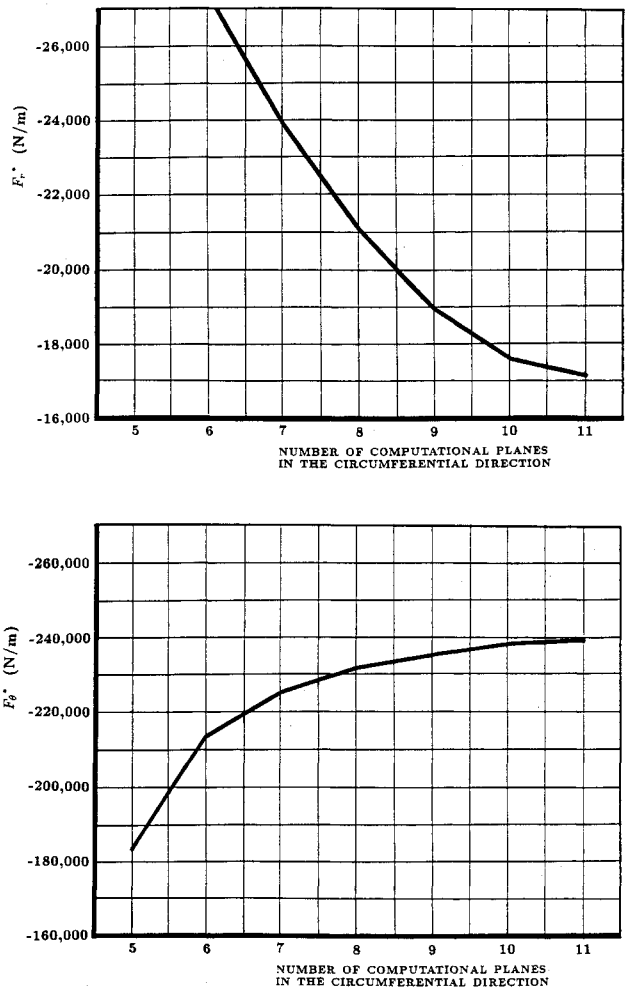

Fig. 13 Dependency of the fluid-exerted forces on the grid resolution in the circumferential direction for the case of synchronous whirl ($\Omega/\omega = 1.0$).

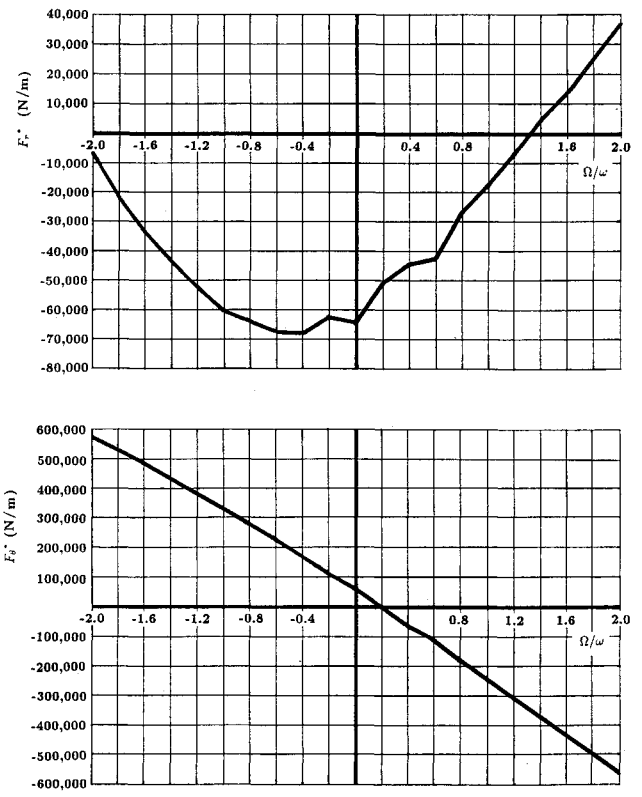

Fig. 14 Fluid-exerted forces on the whirling rotor.

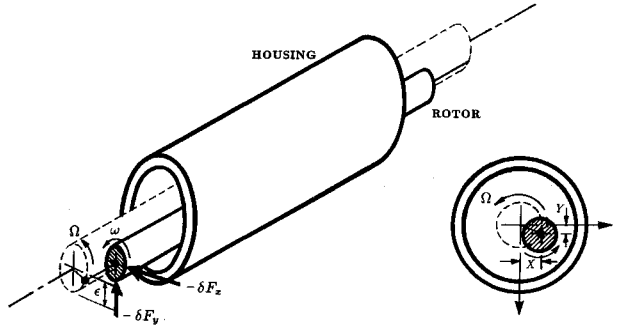

Fig. 15 Components of the rotor whirling motion and the fluid reaction force.

in Fig. 15. The axis location, linear velocity, and acceleration at this position are

$$X = 0 \qquad Y = \varepsilon$$

$$\dot{X} = \Omega\varepsilon \qquad \dot{Y} = 0$$

$$\ddot{X} = 0 \qquad \ddot{Y} = -\Omega^2\varepsilon$$

Substitution of these into the expanded form of the matrix Eq. (2), and taking the limit as ε tends to 0, the following equations are obtained:

$$\frac{\partial F_x}{\partial \varepsilon} = \lim_{\varepsilon \to 0}\left(\frac{\delta F_x}{\varepsilon}\right) = k - \Omega C - \Omega^2 m \tag{3}$$

$$\frac{\partial F_y}{\partial \varepsilon} = \lim_{\varepsilon \to 0}\left(\frac{\delta F_y}{\varepsilon}\right) = -K - \Omega c + \Omega^2 M \tag{4}$$

Determination of the rotordynamic coefficients in Eqs. (3) and (4) requires computation of the derivatives $(\partial F_x/\partial\varepsilon)$ and $(\partial F_y/\partial\varepsilon)$ at a minimum of three different values of Ω. Interpolation of these two derivatives as parabolic expressions of Ω, using curve-fitting techniques, leads to the rotordynamic coefficients by simply equating the different terms in these expressions to those on the right sides of Eqs. (3) and (4).

Contained in Tables 1 and 2 are the computed rotordynamic coefficients of the one- and five-chamber seal configurations, as well as the experimental results of Iwatsubo and Kawai.[5] Missing in these tables are the added-mass (or inertia) coefficients, which were not part of the experimental data. It should be noted, nevertheless, that the computed values of these coefficients were as high as 35.1 and 25.2 kg for the direct and cross-coupled added-mass coefficients, respectively, for the five-chamber seal configuration. As for the tabulated coefficients, the most alarming feature is the poor value of C in both cases. In fact, the negative value of this coefficient, for the single-chamber seal configuration, implies a highly destabilizing effect of this seal, particularly in view of the positive (also destabilizing) value of k in this case.

Although the signs of all the computed rotordynamic coefficients (Tables 1 and 2) are in agreement with their experimental counterparts, the magnitudes of the computed coefficients are vastly different from one data set to the other. Two factors, concerning the seal operating conditions and the accuracy of the experimental measurements, seem to have contributed to these significant differences. First, due to the uncharacteristically low rotor speed and streamwise pressure differential, the rotordynamic coefficients themselves are notably small. Under such circumstances, a measurement inaccuracy that would normally be tolerable may amount to a deviation percentage that is excessively large. Furthermore, the scatter in the experimental data was noted by Iwatsubo and Kawai,[5] who stated that the lack of identifiable patterns

Table 1 Comparison of the rotordynamic coefficients with experimental data for the single-chamber seal configuration

Rotordynamic coefficients	Current perturbation model	Experimental measurements by Iwatsubo and Kawai[5]
K, N/m	6.60×10^4	1.0×10^4
k, N/m	2.20×10^4	0.94×10^4
C, Ns/m	-3.49×10^2	-1.01×10^2
c, Ns/m	-9.19×10^2	-7.75×10^2

Table 2 Comparison of the rotordynamic coefficients with experimental data for the five-chamber seal configuration

Rotordynamic coefficients	Current perturbation model	Experimental measurements by Iwatsubo and Kawai[5]
K, N/m	5.87×10^4	2.30×10^4
k, N/m	6.19×10^4	2.25×10^3
C, Ns/m	1.22×10^4	1.25×10^2
c, Ns/m	-6.60×10^2	-1.75×10^3

in their experimental data may have been caused by the accuracy levels of both the instruments and measurements. It would be natural to suspect that the special set of operating conditions, being the reason of the small magnitudes of the fluid-exerted forces, may have negatively affected the computed coefficients as well. However, it should be noted that the current computational model was executed on a double-precision basis, and that the stability of the matrix inversion step was carefully monitored in order to alleviate any major source of numerical inaccuracy.

Concluding Remarks

The objective of this study was twofold: 1) to demonstrate the applicability of a categorically new perturbation model to the traditionally complex problem of labyrinth-seal rotordynamics; and 2) to assess the stability effects of multiple-chamber seal configurations. Of these, the latter task is largely design-related, and is currently receiving an increasing amount of attention, owing to documented fluid-induced vibration problems in the Space Shuttle Main Engine turbopumps, for which labyrinth seals are primarily blamed. An intermediate outcome of the current study, namely the centered-rotor flowfield, is equally suggestive from a design standpoint. This is true in the sense that knowledge of the flow pattern, for this operation mode, provides a means of predicting the seal effectiveness as a leakage-control device. As for the relative rotordynamic stability, it is the conclusion of this study that increasing the number of chambers in a labyrinth seal imparts a stabilizing effect to the mechanical system. This conclusion is consistent with experimental evidence concerning the incompressible flow seal category.

Acknowledgments

This study was funded by NASA Marshall Space Flight Center, Huntsville, Alabama, Contract NAS8-37821, technical monitor, James Cannon. Partial funding was also provided by the Texas A&M Turbomachinery Research Consortium. The authors are also grateful to David Rhode for his valuable comments and genuine interest in this study.

References

[1]Stoff, H., "Incompressible Flow in a Labyrinth Seal," *Journal of Fluid Mechanics*, Vol. 100, Pt. 4, 1980, pp. 817–829.

[2]Rhode, D. L., Demko, J. A., Morrison, G. L., Traegner, U. K., and Sobolik, S. R., "On the Prediction of Incompressible Flow in Labyrinth Seals," *Journal of Fluids Engineering, Transactions of the American Society of Mechanical Engineers*, Vol. 108, No. 1, 1986, pp. 19–25.

[3]Wittig, S., Schelling, U., Kim, S., and Jacobsen, K., "Numerical Predictions and Measurements of Discharge Coefficients in Labyrinth Seals," American Society of Mechanical Engineers Paper 87-GT-188, 1987.

[4]Rhode, D. L., and Hibbs, R. I., "New Model for Flow over Open Cavities, Part II: Assessment for Seal Leakage," *Journal of Propulsion and Power*, Vol. 8, No. 2, 1992, pp. 398–402.

[5]Iwatsubo, T., and Kawai, R., "Analysis of Dynamic Characteristics of Fluid Force Induced by Labyrinth Seal," *Proceedings of the Workshop on Rotordynamic Instability in High-Performance Turbomachinery*, 1984, pp. 211–234 (NASA 2338).

[6]Zimmermann, H., and Wolff, K. H., "Comparison Between Empirical and Numerical Labyrinth Flow Correlations," American Society of Mechanical Engineers Paper 87-GT-86, 1987.

[7]Alford, J. S., "Protecting Turbomachinery from Self-Excited Rotor Whirl," *Journal of Engineering for Power, Transactions of the American Society of Mechanical Engineers*, 1965, pp. 333–344.

[8]Childs, D., and Elrod, D., "Annular Honeycomb Seals: Test Results for Leakage and Rotordynamic Coefficients; Comparisons to Labyrinth and Smooth Configurations," *Proceedings of the Workshop on Rotordynamic Instability Problems in High-Performance Turbomachinery*, 1988, pp. 143–159 (NASA 3026).

[9]Iwatsubo, T., "Evaluation of Instability Forces of Labyrinth Seals in Turbines or Compressors," *Proceedings of the Rotordynamic Instability Problems in High-Performance Turbomachinery*, NASA 2133, 1980, pp. 139–167.

[10]Childs, D., and Scharrer, J., "An Iwatsubo-Based Solution for Labyrinth Seals, Comparison with Experimental Results," *Journal of Gas Turbines and Power, Transactions of the American Society of Mechanical Engineers*, Vol. 108, No. 2, 1986, pp. 325–331.

[11]Nordmann, R., and Weiser, P., "Rotordynamic Coefficients for Labyrinth Seals Calculated by Means of a Finite Difference Technique," *Proceedings of the Workshop on Rotordynamic Instability in High-Performance Turbomachinery*, 1988, pp. 161–175 (NASA 3026).

[12]Baskharone, E. A., and Hensel, S. J., "A Finite-Element Perturbation Approach to Fluid/Rotor Interaction in Turbomachinery Elements. Part 1: Theory," *Journal of Fluids Engineering, Transactions of the American Society of Mechanical Engineers*, Vol. 113, No. 3, 1991, pp. 362–367.

[13]Baskharone, E. A., and Hensel, S. J., "A Finite-Element Perturbation Approach to Fluid/Rotor Interaction in Turbomachinery Elements. Part 2: Application," *Journal of Fluids Engineering, Transactions of the American Society of Mechanical Engineers*, Vol. 113, No. 3, 1991, pp. 353–361.

[14]Baskharone, E. A., and Hensel, S. J., "Interrelated Rotordynamic Effects of Cylindrical and Conical Whirl of Annular Seal Rotors," *Journal of Tribology, Transactions of the American Society of Mechanical Engineers*, Vol. 113, No. 3, 1991, pp. 470–480.

[15]Morrison, G. L., Johnson, M. C., and Tatterson, G. B., "Three-Dimensional Laser Anemometer Measurements in an Annular Seal," *Journal of Tribology, Transactions of the American Society of Mechanical Engineers*, Vol. 113, No. 3, 1991, pp. 421–427.

[16]Scharrer, J. K., "Rotordynamic Coefficients for Stepped Labyrinth Seals," *Proceedings of the Workshop on Rotordynamic Instability in High-Performance Turbomachinery*, 1988, pp. 177–195 (NASA CP-3026).